MDPI

Article

Ionic Liquid-Assisted Fabrication of Bioactive Heterogeneous Magnetic Nanocatalyst with Antioxidant and Antibacterial Activities for the Synthesis of Polyhydroquinoline Derivatives

Shefa Mirani Nezhad [1], Ehsan Nazarzadeh Zare [1,*], Azimeh Davarpanah [1], Seied Ali Pourmousavi [1], Milad Ashrafizadeh [2] and Alan Prem Kumar [3,4]

[1] School of Chemistry, Damghan University, Damghan 36716-41167, Iran; shefamirani@yahoo.com (S.M.N.); a.d.13962017@gmail.com (A.D.); pourmousavi@du.ac.ir (S.A.P.)
[2] Faculty of Engineering and Natural Sciences, Sabanci University, Orta Mahalle, Üniversite Caddesi No. 27, Orhanlı, Tuzla 34956, Turkey; dvm.milad1994@gmail.com
[3] Cancer Science Institute of Singapore and Department of Pharmacology, Yong Loo Lin School of Medicine, National University of Singapore, Singapore 117599, Singapore; apkumar@nus.edu.sg
[4] NUS Centre for Cancer Research (N2CR), Yong Loo Lin School of Medicine, National University of Singapore, Singapore 117599, Singapore
* Correspondence: ehsan.nazarzadehzare@gmail.com or e.nazarzadeh@du.ac.ir

Abstract: Antibacterial materials have obtained much attention in recent years due to the presence of hazardous agents causing oxidative stress and observation of pathogens. However, materials with antioxidant and antibacterial activities can cause toxicity due to their low biocompatibility and safety profile, urging scientists to follow new ways in the synthesis of such materials. Ionic liquids have been employed as a green and environmentally solvent for the fabrication of electrically conductive polymers. In the present study, an antibacterial poly(p-phenylenediamine)@Fe$_3$O$_4$ (PpPDA@Fe$_3$O$_4$) nanocomposite was fabricated using [HPy][HSO$_4$] ionic liquid. The chemical preparation of PpPDA@Fe$_3$O$_4$ nanocomposite was initiated through the oxidative polymerization of p-phenylenediamine by ammonium persulfate in the presence of [HPy][HSO$_4$]. The PpPDA@Fe$_3$O$_4$ nanocomposite exhibited antibacterial properties against Gram-negative (*Escherichia coli*) and Gram-positive (*Bacillus subtilis*) bacteria. The PpPDA@Fe$_3$O$_4$ nanocomposite was employed as a heterogeneous nanocatalysis for one-pot synthesis of polyhydroquinoline derivatives using aromatic aldehyde, dimedone, benzyl acetoacetate, and ammonium acetate. Polyhydroquinoline derivatives were synthesized in significant yields (90–97%) without a difficult work-up procedure in short reaction times. Additionally, PpPDA@Fe$_3$O$_4$ nanocatalyst was recycled for at least five consecutive catalytic runs with a minor decrease in the catalytic activity. In this case, 11 derivatives of polyhydroquinoline showed in vitro antioxidant activity between 70–98%.

Keywords: magnetic catalyst; ionic liquid; bioactive; antioxidant; antibacterial; polyhydroquinoline derivatives

1. Introduction

The ionic liquids (ILs) are considered substances with a melting point below 100 °C composed of a cation and an anion [1]. The ions present in ILs are tunable and it is possible to develop solvents and catalysts from ILs. The early reports of using ILs in enzymatic reactions were performed in 2000 [2,3]. In addition to chemical synthesis and catalysis, ILs have been employed in electrochemistry, biotechnology, and pharmaceutics [4]. The ILs have been utilized as stabilizers for DNA storage [5]. ILs have been employed in chemical investigations owing to their nonvolatility, high thermal and electrochemical stability [6]. They are environmentally friendly salts that have been employed in the synthesis of organic compounds, catalytic reactions as well as the synthesis of intrinsically conductive polymers (ICPs) [7,8].

Intrinsically conductive polymers (ICPs) such as polyaniline, polypyrrole, and polythiophene, owning to their electrical conductivity, biocompatibility, and environmental stability, have been widely applied in different arenas, e.g., water treatment, catalysts, and biomedical applications [9,10]. Among ICPs, the polyaniline derivatives such as poly(phenylenediamines) (ortho, meta, and para) have attracted special attention. Poly(phenylenediamines) are highly aromatic ladder polymers that exhibited good solubility and poor electrical conductivity compared to polyaniline [11–13]. They have been widely used in water treatment, biosensors, and biomedical applications [14]. In order to improve electrical conductivity, thermal stability, and viscosity of poly(phenylenediamines), ILs can be utilized [15]. Recently, ILs such as 1-alkyl-3-methylimidazolium, 1-butyl-4-methylpyridinium, quaternary ethyltributylammonium, pyridinium carboxylic acid sulfate have been employed for the synthesis of polyaniline and its derivatives [8,11,16,17]. It was reported that ILs played the role of lubricants, plasticizers, interfacial agents in polymer systems, generating enhancements in the mechanical properties, solubility, electrical conductivity, crystallinity, and thermal stability [15].

Iron oxide is an FDA-approved agent significantly applied in nanomedicine [5]. The iron oxide nanomaterials have a diameter of 15–100 nm composed of magnetite or maghemite and have shown great biomedical applications as contrast materials, drug carriers, and thermal-based therapeutics [18]. Iron oxide nanoparticles are under attention because of their excellent properties in polymer-based catalysts [19,20]. This is because iron oxide nanoparticles possess a large surface area for substrate molecules. Furthermore, after the completion of the reactions, the magnetic catalysts can be separated easily from the solution using an external magnet. Additionally, magnetic catalysts can be reused up to numerous runs almost without loss of catalytic activity [21,22].

Several papers have reported the use of P*p*PDA composites as an effective catalyst in organic reactions. For example, Cu_2O-$Cu(OH)_2$/P*p*PDA nanocomposite was used as a high-efficiency catalyst for methanol electrooxidation [23]. P*p*PDA/carbon black composite was employed for oxygen reduction [24]. ZnCr-layered double hydroxides/P*p*PDA/Cu(II) as a catalyst for the synthesis of pyrrole derivatives [25]. In another work, layered double hydroxides/P*p*PDA was applied as an effective catalyst for the synthesis of indolizines [26].

Hantzsch products (e.g., 1,4-dihydropyridine, polyhydroquinoline, and acridine) are products with significant biological activities. They have pharmacological properties, e.g., vasodilator, antihypertensive, bronchodilator, anti-atherosclerotic, hepatoprotective, anti-tumor, anti-mutagenic, neuroprotective, and anti-diabetic [27]. 4-Substituted 1,4-dihydropyridines (1,4-DHPs) establishes a significant class of Ca^{2+} channel blockers [28] and has been used as one of the most important classes of drugs for cardiovascular disease treatment [29]. Polyhydroquinolines have been prepared through conventional heating, microwave irradiation [30], and ultrasound [31].

Herein, we designed a unique organic-inorganic antibacterial and antioxidant nanocatalyst based on P*p*PDA and iron oxide nanoparticles with assisted [HPy][HSO$_4$] using ammonium persulfate as an oxidant. The prepared P*p*PDA@Fe$_3$O$_4$ bioactive nanocomposite was employed as an efficient retrievable eco-friendly catalyst for the synthesis of polyhydroquinoline derivatives through the one-pot four-component reaction of dimedone, benzyl acetoacetate, ammonium acetate, and different aromatic aldehydes under mild reaction conditions (Scheme 1).
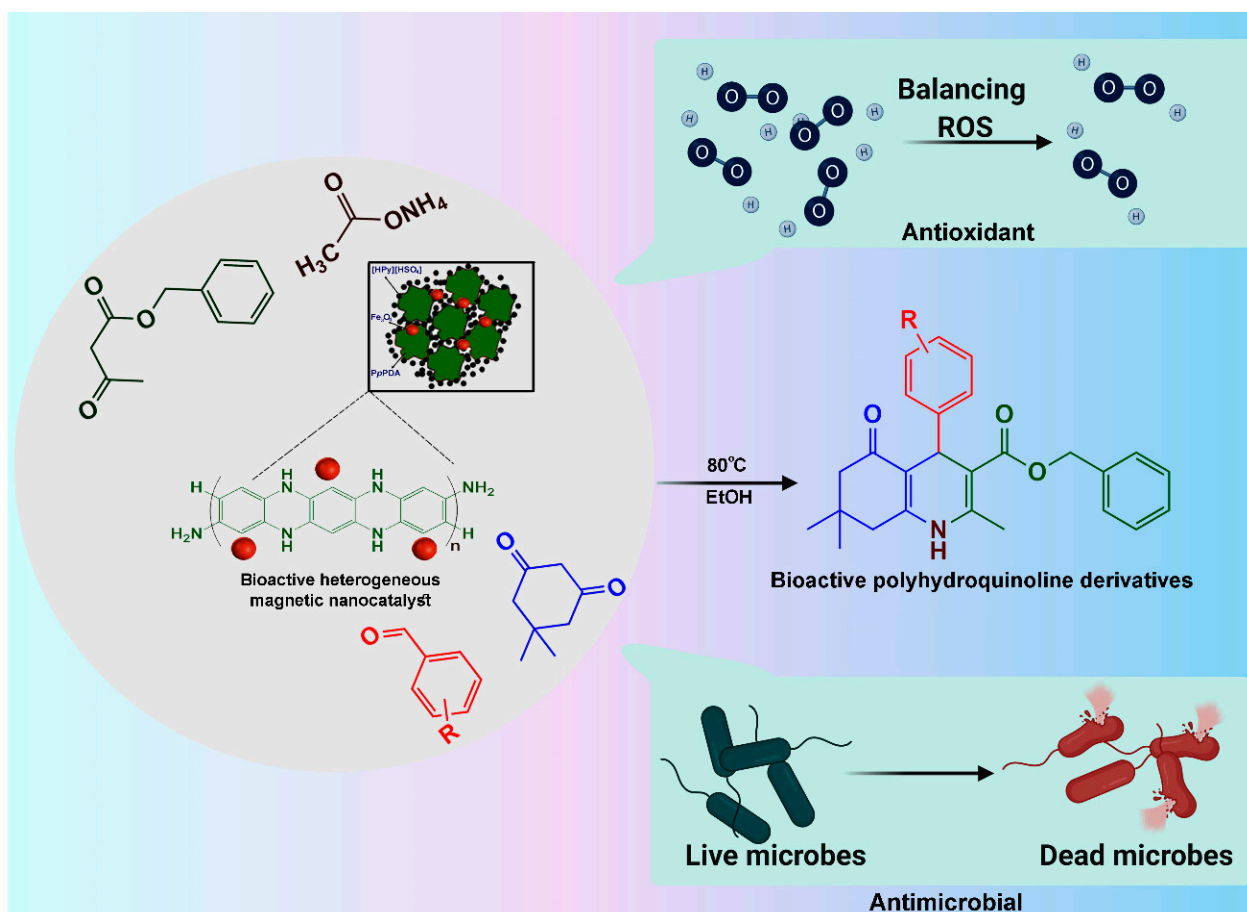
Scheme 1. Schematic illustration of the antibacterial and antioxidant nanocatalyst for synthesis of bioactive polyhydroquinoline derivatives.

2. Results

2.1. Characterization of Polymer-Based Catalyst

FTIR: The FTIR spectra of the prepared P*p*PDA and P*p*PDA@Fe$_3$O$_4$ nanocomposite in the presence of the [HPy][HSO$_4$] ionic liquid are shown in Figure 1a. The P*p*PDA and P*p*PDA@Fe$_3$O$_4$ nanocomposite showed very similar spectra with tiny differences. In the FTIR spectrum of P*p*PDA, the absorption peak at 3200–3450 cm^{-1} is related to the stretching vibration of the NH$_2$ and N-H groups. Two characteristic absorption peaks at 1570 cm^{-1} and 1503 cm^{-1} are associated with the stretching mode of quinoid imine and benzenoid amine units, respectively [32]. The absorption peaks with different intensities in the areas of 1310 cm^{-1}, 1108–1118 cm^{-1}, and 830 cm^{-1} are related to the stretching vibrations of SO$_4$, S=O, and S-OH in the [HPy][HSO$_4$] ionic liquid, respectively [11]. The incorporation of iron oxide nanoparticles in the P*p*PDA matrix led to the appearance of an obvious absorption peak at around 505 cm^{-1} that related to the Fe-O-Fe stretching modes in Fe$_3$O$_4$ [33].

Elemental analysis: Elemental analysis (CHNSO) was employed for characterization of the prepared P*p*PDA and P*p*PDA@Fe$_3$O$_4$ nanocomposite in the presence of the [HPy][HSO$_4$] ionic liquid (Table 1). According to the data in Table 1, the existence of sulfur and oxygen elements in the P*p*PDA approved the presence of [HPy][HSO$_4$] ionic liquid in the structure of the P*p*PDA. The increase of oxygen element in the P*p*PDA@Fe$_3$O$_4$ nanocomposite compared with P*p*PDA shows the presence of Fe$_3$O$_4$ nanoparticles in the nanocomposite [11].
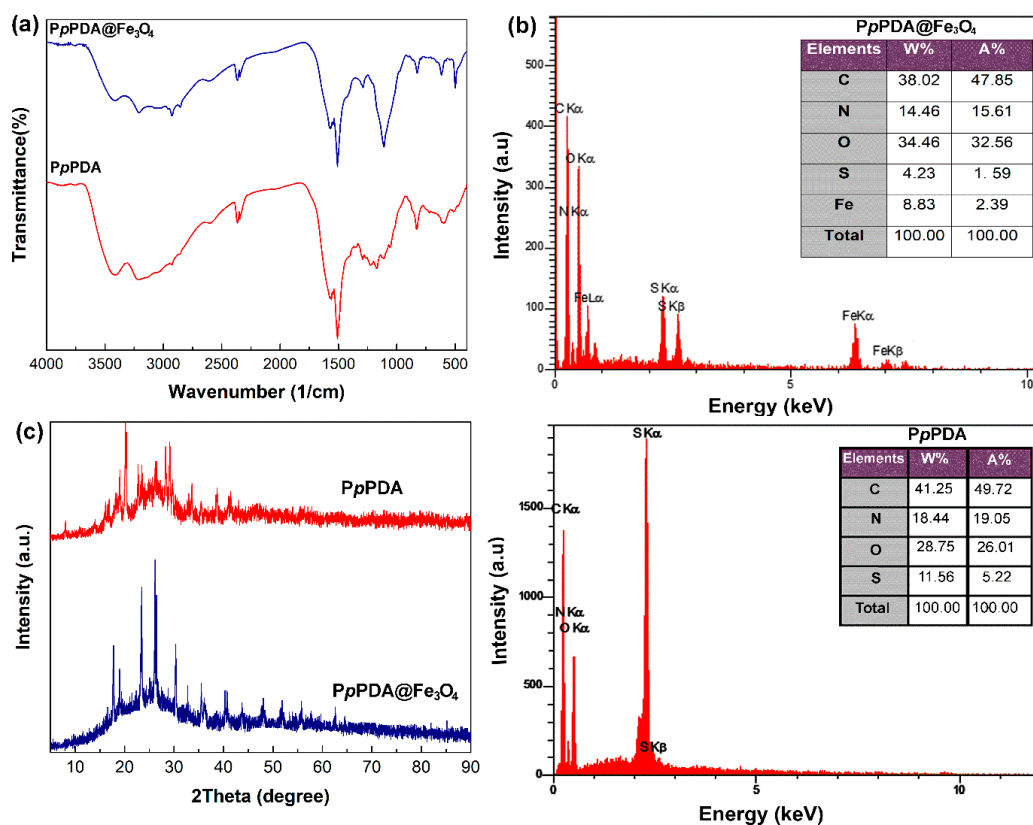
Figure 1. FTIR spectra (**a**), EDX spectra, and tabulated data (**b**) and XRD patterns (**c**) of the prepared P*p*PDA and P*p*PDA@Fe$_3$O$_4$ nanocomposite in the presence of the [HPy][HSO$_4$] ionic liquid.

Table 1. Elemental analysis data of the prepared P*p*PDA and P*p*PDA@Fe$_3$O$_4$ nanocomposite in the presence of the [HPy][HSO$_4$] ionic liquid. Found (Expected).

Samples	C%	H%	N%	S%	O%
P*p*PDA	54.42 (46.31)	2.86 (5.30)	27.4 (14.73)	1.32 (11.24)	14.00 (22.43)
P*p*PDA@Fe$_3$O$_4$	52.00 (46.28)	2.90 (5.27)	26.45 (14.70)	1.25 (11.21)	17.40 (22.55)

EDX: The chemical composition of the prepared P*p*PDA and P*p*PDA@Fe$_3$O$_4$ nanocomposite in the presence of the [HPy][HSO$_4$] ionic liquid was also estimated using the EDX technique as revealed in Figure 1b. The comparison of spectra and tabulated data indicated the existence of different amounts of O, C, N, and S elements. The presence of S in both P*p*PDA and P*p*PDA@Fe$_3$O$_4$ nanocomposite is related to [HPy][HSO$_4$] ionic liquid. In addition, the existence of Fe in the P*p*PDA@Fe$_3$O$_4$ sample indicates the iron oxide in the composite [34].

X-ray diffraction: XRD patterns of the prepared P*p*PDA and P*p*PDA@Fe$_3$O$_4$ nanocomposite in the presence of the [HPy][HSO$_4$] ionic liquid are shown in Figure 1c. According to the literature, the XRD pattern of Fe$_3$O$_4$ nanoparticles indicated a crystalline nature [35]. A semicrystalline nature was observed in the XRD pattern of P*p*PDA owing to intermolecular interactions between the P*p*PDA chains and the [HPy][HSO$_4$] ionic liquid [36]. The XRD pattern of P*p*PDA@Fe$_3$O$_4$ nanocomposite showed more crystallinity compared with P*p*PDA due to the presence of crystalline nanoparticles of Fe$_3$O$_4$ [37].

FESEM: The morphology of Fe$_3$O$_4$ nanoparticles, P*p*PDA, and P*p*PDA@Fe$_3$O$_4$ nanocomposite was investigated using FESEM. The FESEM micrographs of the prepared Fe$_3$O$_4$ nanoparticles (**a**), P*p*PDA (**b**), and P*p*PDA@Fe$_3$O$_4$ nanocomposite (**c**) are shown in Figure 2. The FESEM micrograph of Fe$_3$O$_4$ nanoparticles shows a spherelike structure with a diameter of ~50 nm. Polyhedral shapes with diameters of ~150 nm and ~100 nm observe in the FESEM micrographs of P*p*PDA, and P*p*PDA@Fe$_3$O$_4$ nanocomposite, respectively.
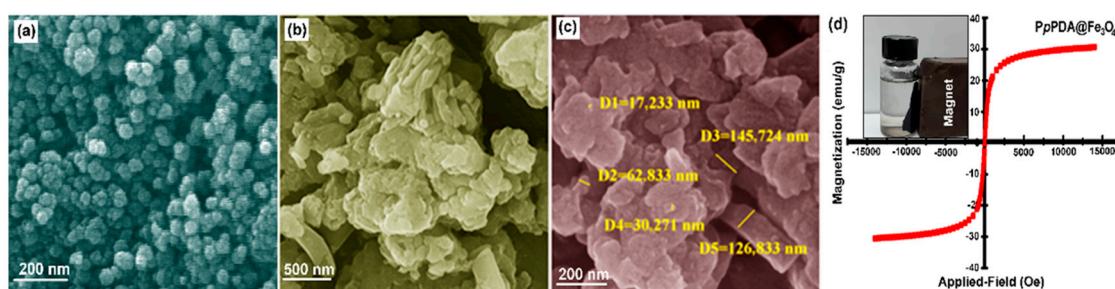
Figure 2. FESEM micrographs of Fe_3O_4 nanoparticles (**a**), P*p*PDA (**b**), and P*p*PDA@Fe_3O_4 nanocomposite (**c**) in the presence of the [HPy][HSO_4] ionic liquid. VSM curve (**d**) of the prepared P*p*PDA@Fe_3O_4 nanocomposite in the presence of the [HPy][HSO_4] ionic liquid.

VSM: Vibrating sample magnetometer (VSM) was employed for the evaluation of the magnetic property of P*p*PDA@Fe_3O_4 nanocomposite as shown in Figure 2d. In the VSM of the P*p*PDA@Fe_3O_4 nanocomposite, the amount of magnetic coercivity (Hc) and magnetic remanence (Mr) is equal to zero. This indicates the P*p*PDA@Fe_3O_4 nanocomposite has a superparamagnetic property with a magnetization saturation value of 30.01 emu/g [38].

Solubility test: The solubility of the prepared P*p*PDA in the presence and absence of [HPy][HSO_4], as well as the P*p*PDA@Fe_3O_4 magnetic nanocomposite prepared in [HPy][HSO_4] in different solvents, were studied (Table 2). The results indicate that the presence of [HPy][HSO_4] improves the solubility of the P*p*PDA. On the other hand, the presence of Fe_3O_4 nanoparticles in P*p*PDA leads to reducing in the solubility of the P*p*PDA.

Table 2. Solubility behavior of the P*p*PDA and P*p*PDA@Fe_3O_4.

| Samples	Solvent					
	H_2O	**MeOH**	**EtOH**	**THF**	**DMF**	**NMP**
P*p*PDA@Fe_3O_4 [a]	--	--	--	--	--	--
P*p*PDA [a]	+-	+-	++	+-	++	++
P*p*PDA [b]	--	+-	+-	--	+-	+-

[a] In presence of [HPy][HSO_4]. [b] In absence of [HPy][HSO_4]. MeOH, Methanol; EtOH, Eehtanol; THF, Tetrahydrofuran; DMF, Dimethylformamide; NMP, *N*-Methyl-2-pyrrolidone (++; Soluble at RT; +-; Partially soluble at RT; –; Insoluble at RT).

2.2. Evaluation of the Catalytic Activity of P*p*PDA@Fe_3O_4 Nanocomposite

In the current study, we offered a new and efficient technique for the synthesis of polyhydroquinolines using P*p*PDA@Fe_3O_4 nanocomposite. We investigated the four-component Hantzsch condensation by aromatic aldehyde, dimedone, benzyl acetoacetate, and ammonium acetate.

The effect of various solvents on the reaction rate and yield of the products was investigated to optimize the reaction conditions.

To optimize the reaction conditions, firstly the various solvents' effect on the rate of reaction and products yield was investigated. The reaction of benzaldehyde (**1**, 1 mmol), dimedon, (**2**, 1 mmol), ammonium acetate (**3**, 1 mmol), and benzyl acetoacetate (**4**, 1 mmol) as a model reaction was catalyzed by 0.03 g of P*p*PDA@Fe_3O_4 in different solvents, e.g., water, ethanol (EtOH), chloroform ($CHCl_3$), tetrahydrofuran (THF) and hexane at reflux conditions (Table 3). In aprotic solvents, e.g., $CHCl_3$, THF, and hexane, the reaction rate was very slow and product yield was low whereas reaction rates, as well as product yields in protic solvents, were improved. In water and solvent-free conditions, the expected product was achieved only in low yield after 4 h. Furthermore, the above condensation reaction by the P*p*PDA@Fe_3O_4 catalyst was also carried out in ethanol at reflux conditions.

Table 3. Optimization of the four-component reaction of dimedone, benzaldehyde, benzyl acetoacetate, and ammonium acetate under various conditions [a].
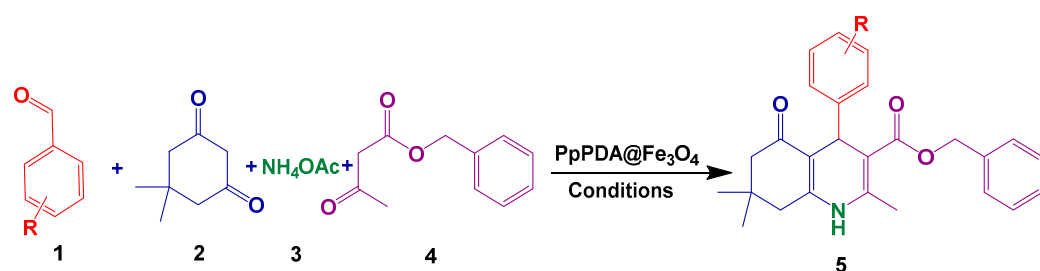
Entry	Solvent	Catalyst (g)	Temp. (°C)	Yield (% [b])	Time (min)
1	EtOH	0.03	Reflux	85	60
2	H_2O	0.03	Reflux	50	240
3	THF	0.03	Reflux	45	240
4	Hexane	0.03	Reflux	20	240
5	$CHCl_3$	0.03	Reflux	40	240
6	-	0.03	80	50	240
7	EtOH	0.03	40	75	240
8	EtOH	0.03	60	80	240
9	EtOH	0.03	R.T.	55	240
10	EtOH	0.04	Reflux	40	60
11	EtOH	0.02	Reflux	60	60
12	EtOH	0.04	Reflux	94	30
13	EtOH	0.06	Reflux	96	30

[a] Reaction conditions: benzaldehyde (1 mmol), dimedone (1 mmol), benzyl acetoacetate (1 mmol), ammonium acetate (1 mmol), solvent (5 mL). [b] Isolated yield.

To optimize the temperature of the reaction, the mixture was heated at various temperatures. The yield of the products was increased when the reaction temperature was raised from room temperature to reflux conditions. Moreover, when 0.02, 0.03, 0.04, and 0.06 of P*p*PDA@Fe$_3$O$_4$ nanocatalyst were used, the yield of the products was 60%, 85%, 94%, and 96%, respectively. Therefore, 0.04 g of P*p*PDA@Fe$_3$O$_4$ was an optimal amount for producing products with high yields. For better comparison, the reaction was also investigated in the absence of the catalyst. Results (Table 3) showed that the rate of reaction was very slow and product yield was low.
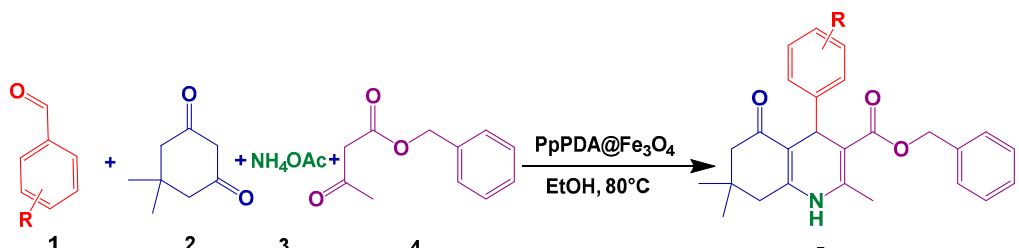
For better comparison, the synthesis of polyhydroquinoline derivatives was studied in the absence and presence of various catalysts, e.g., P*p*PDA, P*p*PDA@[HPy][HSO$_4$], P*p*PDA@Fe$_3$O$_4$@[HPy][HSO$_4$] under the same conditions, and the results are shown in Table 4. The results display that the P*p*PDA@[HPy][HSO$_4$] has better catalytic properties than the P*p*PDA. The major problem of P*p*PDA catalyst is easy solubility in organic solvents and therefore its isolation is difficult. In addition, results showed that the use of 60 mg of P*p*PDA@Fe$_3$O$_4$@[HPy][HSO$_4$] catalyst under the same reaction conditions reduce the reaction time and increased the reaction yield. Consequently, the P*p*PDA@Fe$_3$O$_4$@[HPy][HSO$_4$] nanocatalyst was selected as an effective catalyst to perform the reactions.

Table 5 shows that aromatic aldehydes containing electron-donating and electron-withdrawing groups reacted with dimedone, benzyl acetoacetate, and ammonium acetate in the presence of P*p*PDA@Fe$_3$O$_4$ magnetic nanocatalyst in optimal conditions and in a short time to produced polyhydroquinolines with excellent yields. Likewise, thiophene-carbaldehyde and furfural (heteroaromatic aldehydes) produced the desired product after 35 min with 92% and 90% yields respectively (Table 5, entries 12 and 14). P*p*PDA@Fe$_3$O$_4$ magnetic nanocatalyst was also suitable for the synthesis of polyhydroquinolines from aliphatic aldehyde such as α-methyl cinnamaldehyde (Table 5, entry 13). Dialdehydes such as para phenylene dialdehyde and 2,2′-(hexane-1,6-diylbis(oxy))dibenzaldehyde reacted under optimal conditions using P*p*PDA@Fe$_3$O$_4$ magnetic nanocatalyst and produced products with high yields (Table 5, entries 23 and 24).

Table 4. Influence of the catalyst in the synthesis of polyhydroquinoline derivatives under various conditions [a].

Entry	Catalyst	Catalyst (g)	Temp. (°C)	Time (min)	Yield (% [b])
1	Without catalyst	-	Reflux	60	40
2	PpPDA in the absence [HPy][HSO$_4$]	0.04	Reflux	60	90
3	PpPDA in the presence of [HPy][HSO$_4$]	0.04	Reflux	25	95
4	PpPDA@Fe$_3$O$_4$	0.04	Reflux	30	94
5	PpPDA@Fe$_3$O$_4$	0.02	Reflux	60	60
6	PpPDA@Fe$_3$O$_4$	0.03	Reflux	60	85
7	PpPDA@Fe$_3$O$_4$	0.06	Reflux	30	96

[a] Reaction of benzaldehyde (1 mmol), dimedone (1 mmol), benzyl acetoacetate (1 mmol), and ammonium acetate (1 mmol), ethanol (5 mL) under reflux conditions. [b] Isolated yield.

Table 5. Conversion of benzaldehyde derivatives to polyhydroquinolines in the presence of PpPDA@Fe$_3$O$_4$ magnetic nanocatalyst [a].
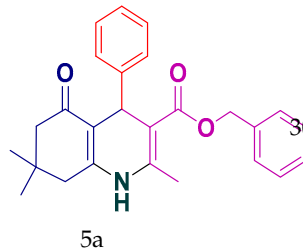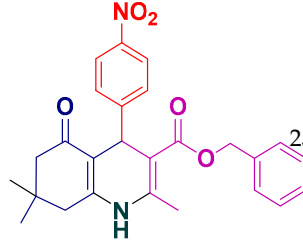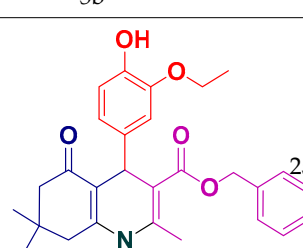

Entry	Product	Time (min)	Yield % [b]	Observed M.P (°C)
1	5a	30	94	172–174
2	5b	25	94	148–150
3	5c	25	97	210–212

Table 5. *Cont.*

Entry	Product	Time (min)	Yield % [b]	Observed M.P (°C)
4	5d	20	93	135–137
5	5e	20	92	140–142
6	5f	25	94	160–162
7	5g	30	93	130–132
8	5h	30	95	154–156
9	5i	35	90	169–171

Table 5. *Cont.*
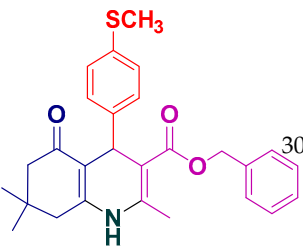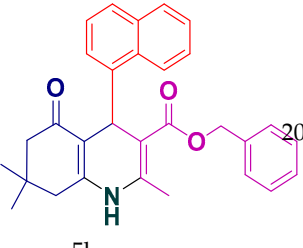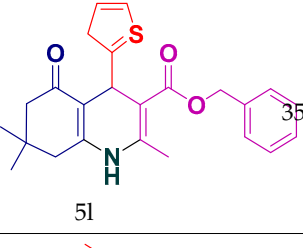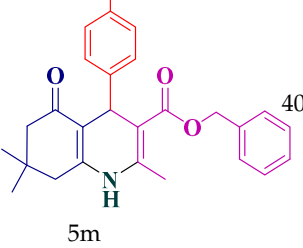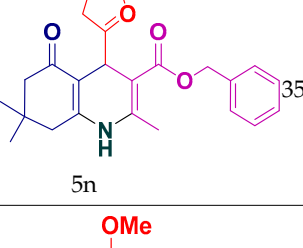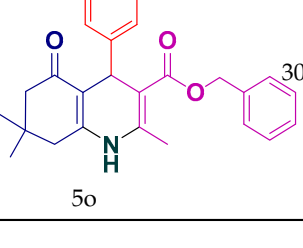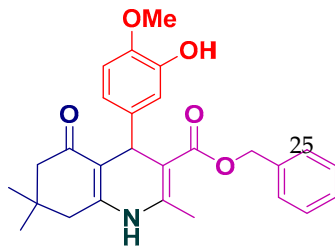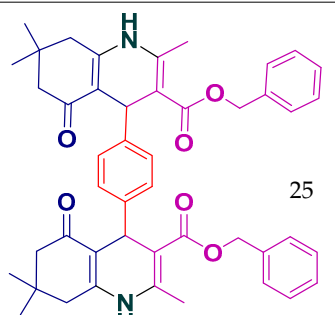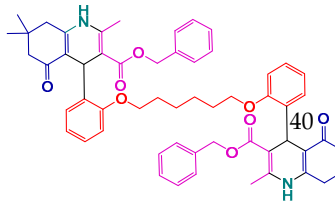
Entry	Product	Time (min)	Yield % [b]	Observed M.P (°C)
10	5j	30	92	126–128
11	5k	20	96	200–202
12	5l	35	92	216–218
13	5m	40	90	165–167
14	5n	35	90	188–190
15	5o	30	91	151–153 (187–189) [39]

Table 5. *Cont.*

Entry	Product	Time (min)	Yield % [b]	Observed M.P (°C)
16	5p	20	92	147–149
17	5q	20	94	219–221
18	5r	20	96	178–180
19	5s	30	93	212–214
20	5t	30	90	248–250
21	5u	35	92	212–215

Table 5. *Cont.*

Entry	Product	Time (min)	Yield % [b]	Observed M.P (°C)
22	5v	25	94	141–143
23	5w	25	95	327–330
24	5x	40	92	161–163

[a] Reaction conditions: aldehyde (1 mmol), dimedone (1 mmol), benzyl acetoacetate (1 mmol), ammonium acetate (1 mmol), ethanol (5 mL) and PpPDA@Fe$_3$O$_4$ (0.04 g) under reflux conditions. [b] Isolated yield.

Proposed mechanistic scheme: The PpPDA@Fe$_3$O$_4$ nanocomposite with active sites such as base (secondary amines in polymer backbone), Brønsted acid ([HPy][HSO$_4$], Lewis acid site (Fe^{3+} in Fe$_3$O$_4$), and large surface area, play a significant role in all steps of reactions as demonstrated in Figure 3. First, dimedone is activated in the presence of amine groups in PpPDA, and then, as a nucleophile, attacks the aldehyde activated by the [HPy][HSO$_4$] to form intermediate (I) (Knoevenagel condensation). On the other hand, ammonium acetate is converted to acetic acid and ammonia, and then the ammonia as a nucleophile attacks the benzyl acetate activated by the [HPy][HSO$_4$] to form intermediate (II). In the next step, Michael's addition reaction of intermediate (II) to intermediate (I) causes the formation of intermediate (III). The intermediate (III) is then converted to the intermediate (IV) by tautomerization and the product (VI) is obtained after cyclization reaction.

Recovery and reusability: Recyclability is an important property of heterogeneous catalytic systems in terms of environmental protection and industrial application. To evaluate the reusability of PpPDA@Fe$_3$O$_4$, it was magnetically isolated from the reaction mixture, washed several times with distilled water and ethanol, dried at room temperature, utilized again in the next reaction. As is observed in Figure 4, the yield of the products was not reduced considerably after five successive catalytic runs and the catalyst has retained its efficacy and stability in the synthesis of polyhydroquinolines derivatives.
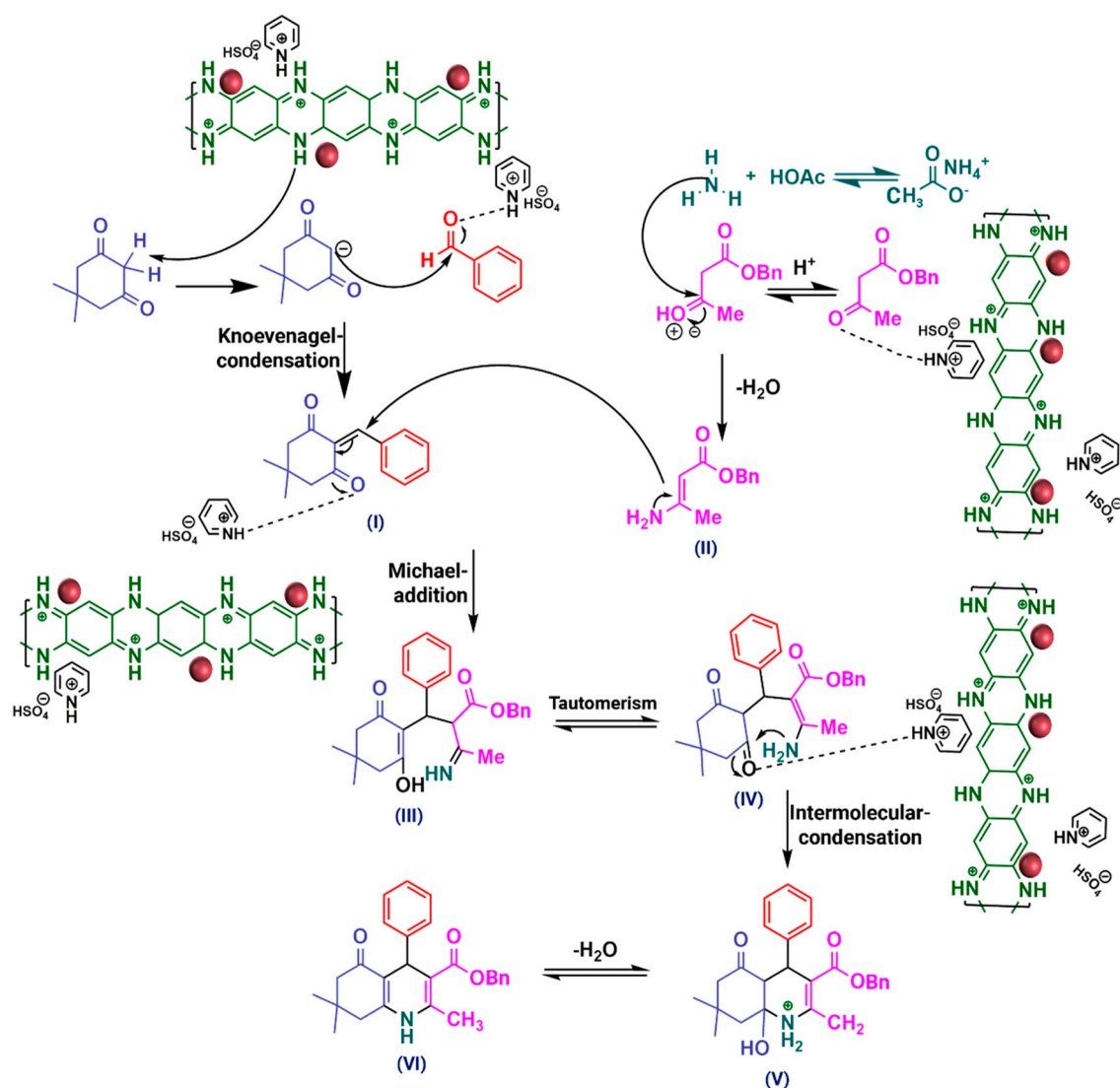
Figure 3. Proposed mechanistic scheme for the synthesis of polyhydroquinolines derivatives catalyzed by P*p*PDA@Fe$_3$O$_4$ nanocomposite. Note: The relative size of nanoparticles and chemical structures in the scheme is assumptive.
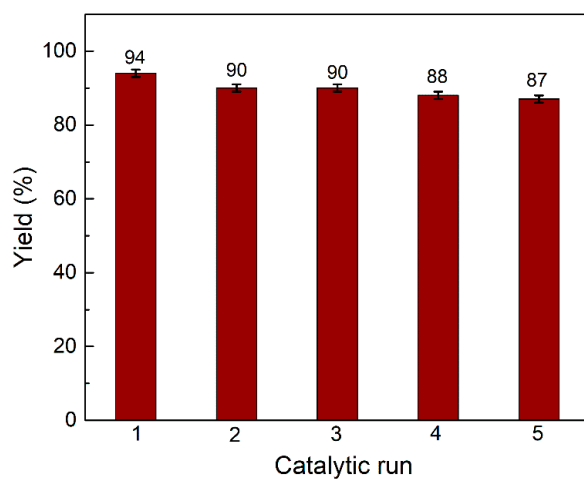

Figure 4. The Reusability of P*p*PDA@Fe$_3$O$_4$ in the synthesis of polyhydroquinoline derivatives.

Antioxidant activity: The antioxidant activity of Fe$_3$O$_4$ NPs, PpPDA, PpPDA@[HPy][HSO$_4$], PpPDA@Fe$_3$O$_4$@[HPy][HSO$_4$], and synthesized polyhydroquinoline derivatives was studied using the 2,2-diphenyl-1-picrylhydrazyl (DPPH)radical scavenging model (Figure 5). Results showed that all used materials to prepare magnetic nanocatalysts had antioxidant activities between 72% and 90%. In addition, the antioxidant activity of 24 synthesized derivatives was investigated. Only 11 derivatives showed antioxidant activity between 75% and 98%. These results suggest that these derivatives may play a role in the synthesis of immune-boosting drugs.
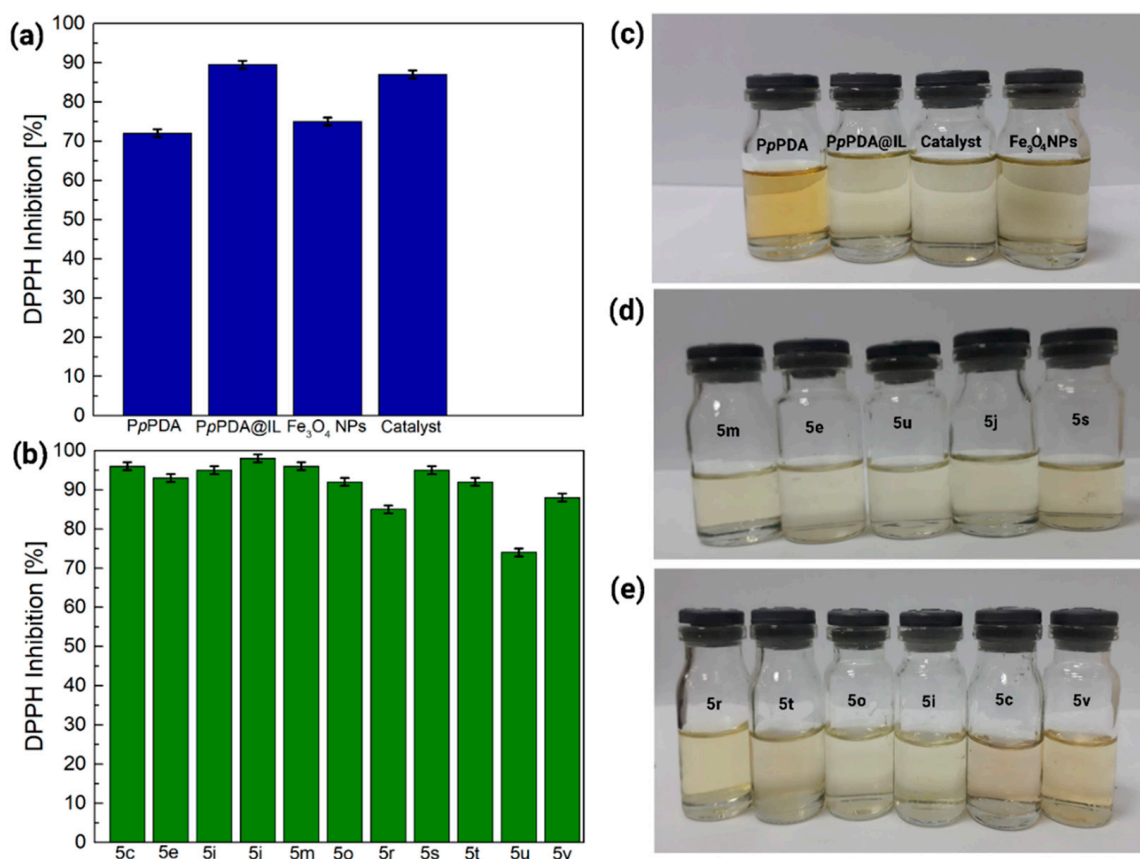
Figure 5. The histograms (**a**,**b**) and the photographs (**c**–**e**) of antioxidant activity of Fe$_3$O$_4$ NPs, PpPDA, PpPDA@[HPy][HSO$_4$], PpPDA@Fe$_3$O$_4$@[HPy][HSO$_4$], and synthesized polyhydroquinoline derivatives.

Antibacterial activity: The *in vitro* antibacterial activities of the Fe$_3$O$_4$ NPs, PpPDA, PpPDA@[HPy][HSO$_4$] (PpPDA@IL), PpPDA@Fe$_3$O$_4$@[HPy][HSO$_4$] (nanocatalyst), and seven of polyhydroquinoline derivatives (5c, 5i, 5j, 5r, 5s, 5o, and 5v) were investigated against *Escherichia coli* and *Bacillus subtilis*, and results shown in Table 6 and Figure 6. The results showed that the bare PpPDA and Fe$_3$O$_4$ NPs had good growth inhibitory effects against tested microorganisms, and among them, Fe$_3$O$_4$ NPs exhibited the highest antibacterial activity against both microorganisms while PpPDA@IL was effective against *Bacillus subtilis*. The nanocatalyst showed lower antimicrobial activity than that of bare minerals against tested bacteria. Moreover, among polyhydroquinoline derivatives, only 5r and 5v had good growth inhibitory effects against tested microorganisms while 5i and 5o showed no effect against tested microorganisms.

Table 6. Antibacterial activities data of catalysts and some polyhydroquinoline derivatives via Kirby–Bauer disc diffusion technique.

		Inhibition Zone (mm)	
Entry	Compound	*Bacillus subtilis* Gram-Positive (+)	*Escherichia coli* Gram-Negative (−)
1	Fe_3O_4 NPs	24 ± 1.2	25 ± 1.2
2	P*p*PDA@IL	9 ± 0.6	NE [a]
3	P*p*PDA	20 ± 1.2	22 ± 1.7
4	Nanocatalyst	9 ± 0.6	8 ± 0.6
5	5c	8 ± 0.6	NE
6	5i	NE	NE
7	5j	10 ± 1.0	NE
8	5o	NE	NE
9	5r	12 ± 1.0	12 ± 1.0
10	5s	9 ± 0.7	NE
11	5v	11 ± 0.7	10 ± 1.0
12	Gentamicin	26 ± 1.2	19.6 ± 0.7
13	Chloramphenicol	22.3 ± 1.7	20.7 ± 1.0

[a] No effect.
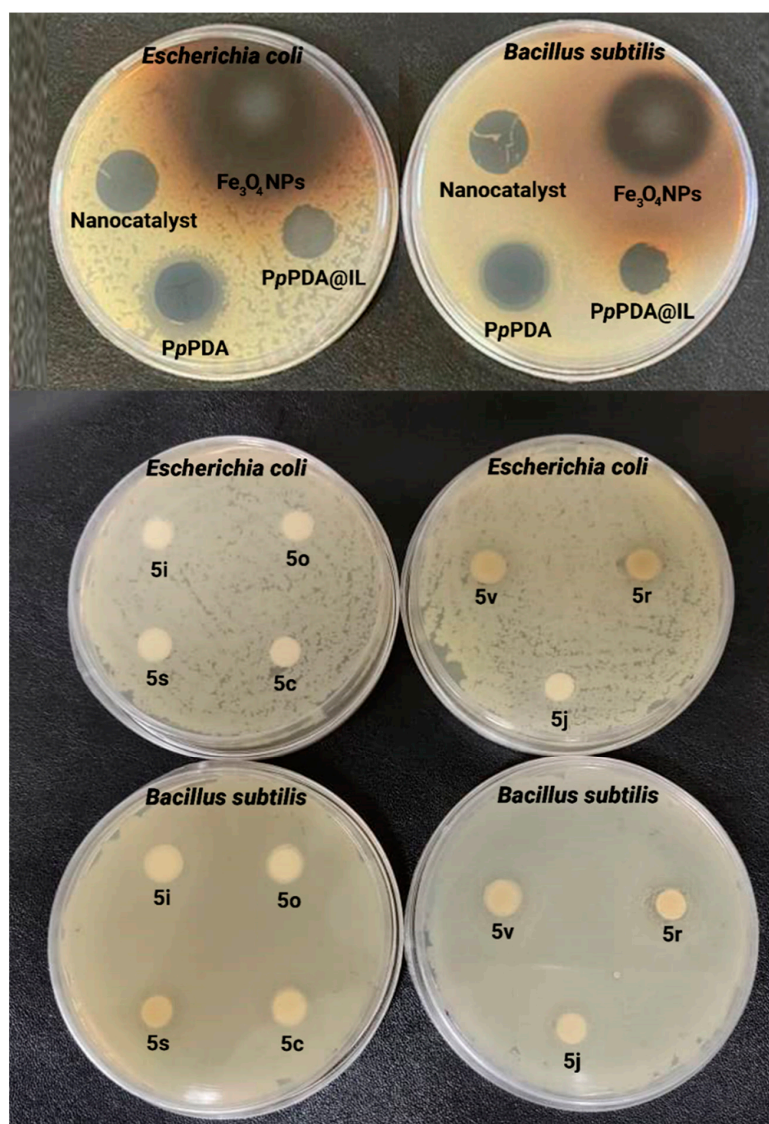
Figure 6. Antibacterial activities of catalysts and some polyhydroquinoline derivatives against *Escherichia coli* and *Bacillus subtilis* via Kirby–Bauer disc diffusion technique.

Spectroscopic Data (^{1}H-NMR and ^{13}C-NMR of products are shown in Supplementary Materials)

Benzyl2,7,7-trimethyl-4-(4-nitrophenyl)-5-oxo-1,4,5,6,7,8-hexahydroquinoline-3-carboxylate (Table 5, Entry 2, Figures S1 and S2)

Solid, m.p.148–150 °C. ^{1}H NMR (400 MHz, DMSO-d_6): δ (ppm) 0.80 (s, 3H, CH$_3$), 1.00 (s, 3H, CH$_3$), 1.97 (d, 1H, *J* = 16 Hz, CH$_2$), 2.18 (d, 1H, *J* = 16 Hz, CH$_2$), 2.32 (s, 3H, CH$_3$), 2.27–2.246 (m, 2H, CH$_2$), 4.96–5.61 (m, 1H, benzilic, OCH$_2$ benzilic), 7.16–7.37 (m, 7H, aromatic), 8.04 (d, 2H, *J* = 8 Hz), 9.33 (s, 1H, NH), ^{13}C-NMR (100 MHz, DMSO-d_6): δ (ppm) 18.93, 26.87, 29.46, 32.62, 37.06, 40.58, 45.41, 50.50, 65.38, 102.34, 109.59, 123.63, 128.29, 128.73, 129.25, 136.93, 146.07, 147.44, 150.47, 155.27, 166.61, 194.77.

Benzyl4-(3-ethoxy-4-hydroxyphenyl)-2,7,7-trimethyl-5-oxo-1,4,5,6,7,8-hexahydroquinoline-3-carboxylate (Table 5, Entry 3, Figures S3 and S4)

Solid, m.p.209–211 °C. ^{1}H NMR (400 MHz, DMSO-d_6): δ (ppm) 0.85(s, 3H, CH$_3$), 1.00 (s, 3H, CH$_3$), 1.24 (t, 3H, *J* = 6.8 Hz CH$_3$), 1.97 (d, 1H, *J* = 16.4 Hz, CH$_2$), 2.13 (d, 1H, *J* = 16.4 Hz, CH$_2$), 2.29 (s, 3H, CH$_3$), 2.24–2.29 (m, 2H, CH$_2$), 2.41(d, 2H, *J* = 17.2 Hz, CH$_2$), 4.77 (s, 1H, benzilic), 5.33 (AB q, 2H, *J* = 12 Hz, OCH$_2$ benzilic), 6.46–6.63 (m, 3H, aromatic), 7.22–7.33 (m, 5H, aromatic), 8.56 (s, 1H, OH) 9.07 (s, 1H, NH), ^{13}C-NMR (100 MHz, DMSO-d_6): δ (ppm) 15.23, 18.58, 26.82, 29.67, 32.60, 35.41, 50.76, 64.06, 65.22, 103.90, 110.92, 113.96, 115.49, 120.06, 128.11, 128.16, 128.75, 137.19, 139.30, 145.29, 145.84, 146.23, 149.52, 167.28, 194.88.

Benzyl2,7,7-trimethyl-5-oxo-4-(3,4,5-trimethoxyphenyl)-1,4,5,6,7,8-hexahydroquinoline-3-carboxylate (Table 5, Entry 5, Figures S5 and S6)

Solid, m.p.140–142 °C. ^{1}H NMR (400 MHz, DMSO-d_6): δ (ppm) 0.91 (s, 3H, CH$_3$), 1.02 (s, 3H, CH$_3$), 2.02 (d, 1H, *J* = 16 Hz, CH$_2$), 2.19 (d, 1H, *J* = 15.6 Hz, CH$_2$), 2.31 (s, 3H, CH$_3$), 2.31–2.47 (m, 2H, CH$_2$), 3.37 (s, 6H, OCH$_3$), 3.55 (s, 3H, OCH$_3$), 4.86 (s, 1H, benzilic), 5.08 (AB q, 2H, *J* = 12 Hz, OCH$_2$ benzilic), 6.37 (s, 2H, aromatic), 7.25–7.33 (m, 5H, aromatic), 9.17 (s, 1H, NH). ^{13}C-NMR (100 MHz, DMSO-d_6): δ (ppm) 18.90, 19.03, 21.51, 26.75, 29.70, 31.62, 32.61, 36.20, 50.70, 55.98, 60.33, 65.29, 66.07, 103.57, 105.05, 110.37, 126.87, 127.61, 127.85, 128.22, 128.79, 136.13, 137.21, 143.75, 146.30, 150.13, 167.19, 172.53, 194.96.

Benzyl2,7,7-trimethyl-5-oxo-4-(p-tolyl)-1,4,5,6,7,8-hexahydroquinoline-3-carboxylate (Table 5, Entry 9, Figures S7 and S8)

Solid, m.p.165–167 °C. ^{1}H-NMR (400 MHz, DMSO-d_6): δ (ppm) 0.83 (s, 3H, CH$_3$), 1.00 (s, 3H, CH$_3$), 1.96 (d, 1H, *J* = 16 Hz, CH$_2$), 2.13 (d, 1H, *J* = 16 Hz, CH$_2$), 2.20 (s, 3H, CH$_3$), 2.25 (s, 3H, CH$_3$), 2.25–2.39 (m, 2H, CH$_2$), 2.41(d, 2H, *J* = 30 Hz, CH$_2$), 4.84 (s, 1H, benzilic), 5.01 (AB q, 2H, *J* = 12.8 Hz, OCH$_2$ benzilic), 6.96 (d, 2H, *J* = 8 Hz, aromatic), 7.01 (d, 2H, *J* = 8 Hz, aromatic), 7.19–7.32 (m, 5H, aromatic), 9.12 (s, 1H, NH), ^{13}C-NMR (100 MHz, DMSO-d_6): δ (ppm) 18.87, 21.07, 21.78, 26.90, 29.61, 32.60, 35.20, 39.32, 46.93, 50.70, 65.22, 103.68, 110.72, 128.18, 128,74, 135.07, 137.14, 145.11, 146.12, 149.70, 167.12, 172.73, 194.77.

Benzyl2,7,7-trimethyl-5-oxo-4-(p-tolyl)-1,4,5,6,7,8-hexahydroquinoline-3-carboxylate (Table 5, Entry 10, Figures S9 and S10)

Solid, m.p.126–128 °C. ^{1}H NMR (400 MHz, DMSO-d_6): δ (ppm) 0.83 (s, 3H, CH$_3$), 1.00 (s, 3H, CH$_3$), 1.97 (d, 1H, *J* = 15.6 Hz, CH$_2$), 3.94 (d, 1H, *J* = 16.4 Hz, CH$_2$), 2.30 (s, 3H, CH$_3$), 2.41 (s, 3H, SCH$_3$), 2.25–2.42 (m, 2H, CH$_2$), 2.53 (d, 2H, *J* = 20 Hz, CH$_2$), 4.83 (s, 1H, benzilic), 5.02 (AB q, 2H, *J* = 12 Hz, OCH$_2$ benzilic), 7.06–7.30 (m, 9H, aromatic), 9.15 (s, 1H, NH), ^{13}C-NMR (100 MHz, DMSO-d_6): δ (ppm) 15.31, 18.88, 26.95, 29.57, 32.62, 35.85, 50.67, 65.23,

103.41, 110.47, 125.62, 126.08, 128.18, 128.64, 128.75, 135.30, 137.12, 144.90, 146.320, 146.80, 167.02, 194.79.

Benzyl4-(4-ethylphenyl)-2,7,7-trimethyl-5-oxo-1,4,5,6,7,8-hexahydroquinoline-3-carboxylate (Table 5, Entry 13, Figures S11 and S12)

Solid, m.p.165–167 °C. ^{1}H NMR (400 MHz, DMSO-d_6): δ (ppm) 0.84 (s, 3H, CH$_3$), 1.00 (s, 3H, CH$_3$), 1.13 (t, 3H, J = 8 Hz, CH$_3$), 1.97 (d, 1H, J = 15.6 Hz, CH$_2$), 2.15 (d, 1H, J = 16.4 Hz, CH$_2$), 2.29 (s, 3H, CH$_3$), 2.26–2.48 (m, 2H, CH$_2$), 4.84 (s, 1H, benzilic), 5.02 (AB q, 2H, J = 12 Hz, OCH$_2$ benzilic), 7.01 (dd, 4H, J = 8, 15.6 aromatic),7.18–7.41 (m, 4H, aromatic) 9.11 (s, 1H, NH), ^{13}C-NMR (100 MHz, DMSO-d_6): δ (ppm) 16.09, 18.90, 27.01, 28.23, 29.57, 32.62, 35.81, 50.72, 65.21, 103.74, 110.71, 127.60, 127.94, 128.16, 128.72, 137.17, 141.43, 145.38, 146.11, 149.75, 167.13, 194.77.

Benzyl4-(3,4-dimethoxyphenyl)-2,7,7-trimethyl-5-oxo-1,4,5,6,7,8-hexahydroquinoline-3-carboxylate (Table 5, Entry15, Figure S13)

Solid, m.p.151–153–167 °C. ^{1}H NMR (400 MHz, DMSO-d_6): δ (ppm) 0.86 (s, 3H, CH$_3$), 1.01 (s, 3H, CH$_3$), 1.99 (d, 1H, J = 16 Hz, CH$_2$), 2.17 (d, 1H, J = 16.4 Hz, CH$_2$), 2.31 (s, 3H, CH$_3$), 2.19–2.50 (m, 2H, CH$_2$), 247 (d, 2H, J = 24 Hz, CH$_2$), 3.53 (s, 3H, OCH$_3$), 3.67 (s, 3H, OCH$_3$), 4.84 (s, 1H, benzilic), 5.04 (AB q, 2H, J = 12 Hz, OCH$_2$ benzilic), 6.61 (dd, 1H, J = 2 Hz, 8 Hz, H aromatic), 6.70–6.76 (m, 2H, aromatic), 7.22–7.24 (m, 2H, aromatic), 7.29–7.32 (m, 3H, aromatic) 9.14 (s, 1H, NH).

Benzyl4-(2-chlorophenyl)-2,7,7-trimethyl-5-oxo-1,4,5,6,7,8-hexahydroquinoline-3-carboxylate (Table 5, Entry 18, Figures S14 and S15)

Solid, m.p.178–180 °C. ^{1}H NMR (400 MHz, DMSO-d_6): δ (ppm) 0.84(s, 3H, CH$_3$), 1.00 (s, 3H, CH$_3$), 1.91 (d, 1H, J = 16 Hz, CH$_2$), 2.14 (d, 1H, J = 16 Hz, CH$_2$), 2.28 (s, 3H, CH$_3$), 2.25–2.240 (m, 2H, CH$_2$), 4.99 (AB q, 2H, J = 12 Hz, OCH$_2$ benzilic), 5.21 (s, 1H, benzilic), 7.08–7.27 (m, 9H, aromatic), 9.17 (s, 1H, NH), ^{13}C-NMR (100 MHz, DMSO-d_6): δ (ppm) 18.86, 21.70, 26.82, 29.61, 32.44, 35.49, 46.87, 50.69, 56.52, 56.03, 101.83, 103.14, 110.13, 127.72,128.09, 128.65, 129.56, 132.07, 132.56, 137.27, 145.47, 146.37, 150.12, 166.99, 172.64, 194.41.

Benzyl4-(3-hydroxyphenyl)-2,7,7-trimethyl-5-oxo-1,4,5,6,7,8-hexahydroquinoline-3-carboxylate (Table 5, Entry 19, Figures S16 and S17)

Solid, m.p.212–214 °C. ^{1}H NMR (400 MHz, DMSO-d_6): δ (ppm) 0.85 (s, 3H, CH$_3$), 1.00 (s, 3H, CH$_3$), 1.97 (d, 1H, J = 16 Hz, CH$_2$), 2.13 (d, 1H, J = 16 Hz, CH$_2$), 2.30 (s, 3H, CH$_3$), 2.24–2.230 (m, 2H, CH$_2$), 4.89 (s, 1H, benzilic), 5.04 (AB q, 2H, J = 12Hz, OCH$_2$ benzilic), 6.48 (dd, 1H, J = 1.6 Hz, 8 Hz, aromatic), 7.56–6.61 (m, 2H, aromatic), 6.94 (t, 1H, J = 8 Hz, aromatic), 7.18–7.21 (m, 2H, aromatic), 7.28–7.31 (m, 4H, aromatic, OH), 9.11 (s, 1H, NH), ^{13}C-NMR (100 MHz, DMSO-d_6): δ (ppm) 18.91, 26.99, 29.57, 32.61, 35.96, 50.75, 56.51, 65.17, 103.45, 110.60, 113.16, 113.16, 115.02, 118.73, 128.01, 128.10, 128.76, 1129.03, 137.21, 146.18, 149.25, 149.74, 157.42, 167.17, 194.79.

Benzyl4-(2-hydroxy-3-methoxyphenyl)-2,7,7-trimethyl-5-oxo-1,4,5,6,7,8-hexahydroquinoline-3-carboxylate (Table 5, Entry 20, Figures S18 and S19)

Solid, m.p.248–250 °C. ^{1}H NMR (400 MHz, DMSO-d_6): δ (ppm) 0.78 (s, 3H, CH$_3$), 1.01 (s, 3H, CH$_3$), 2.09 (d, 1H, J = 16 Hz, CH$_2$), 2.15 (d, 1H, J = 16 Hz, CH$_2$), 2.41–2.45 (m, 5H, CH$_2$ CH$_3$), 3.70 (s, 3H, OCH$_3$), 4.97 (AB q, 2H, J = 13.2 Hz, OCH$_2$ benzilic), 5.08 (s, 1H, benzilic), 6.54 (dd, 1H, J = 1.6 Hz, 7.6 Hz, H aromatic), 6.65–6.73 (m, 2H, aromatic), 6.99–7.01 (m, 2H, aromatic), 7.19–7.23 (m, 3H, aromatic), 9.26 (s, 1H, OH), 9.43 (s, 1H, NH).

Benzyl4-(3-hydroxy-4-methoxyphenyl)-2,7,7-trimethyl-5-oxo-1,4,5,6,7,8-hexahydroquinoline-3-carboxylate (Table 5, Entry 22, Figure S20)

Solid, m.p.141–143 °C. ^{1}H NMR (400 MHz, DMSO-d_6): δ (ppm) 0.85 (s, 3H, CH$_3$), 1.00 (s, 3H, CH$_3$), 1.98 (d, 1H, J = 16 Hz, CH$_2$), 2.24–2.41 (m, 6H, CH$_2$, CH$_3$), 3.68 (s, 3H, OCH$_3$), 4.78 (s, 1H, benzilic), 5.03 (AB q, 2H, J = 13.6 Hz, OCH$_2$ benzilic), 6.51(dd, 1H, J = 2 Hz, 8.4 Hz, H aromatic), 6.62–6.70 (m, 2H, aromatic), 7.19–7.21 (m, 2H, aromatic), 7.28–7.31 (m, 3H, aromatic), 8.68 (s, 1H, OH), 9.08 (s, 1H, NH), ^{13}C-NMR (100 MHz, DMSO-d_6): δ (ppm) 18.89, 27.03, 29.58, 32.60, 35.31, 50.78, 56.02, 65.13, 103.78, 110.83, 112.05, 115.61, 118.54, 128.01, 128.09, 128.75, 137.24, 140.86, 145.81, 146.18, 146.30, 149.45, 167.25, 194.83.

Dibenzyl4,4′-(1,4-phenylene)bis(2,7,7-trimethyl-5-oxo-1,4,5,6,7,8-hexahydroquinoline-3-carboxylate) (Table 5, Entry 23, Figures S21 and S22)

Solid, m.p.327–330 °C. ^{1}H NMR (400 MHz, DMSO-d_6): δ (ppm) 0.81(s, 3H, CH$_3$), 0.98 (s, 3H, CH$_3$), 1.98 (d, 1H, J = 16 Hz, CH$_2$), 2.10–2.15 (m, 1H, J = 16 Hz, CH$_2$), 2.30 (s, 3H, CH$_3$), 2.29–2.236 (m, 2H, CH$_2$), 4.84 (s, 1H, benzilic), 4.99 (AB q, 2H, J = 12 Hz, OCH$_2$ benzilic), 6.89–6.90 (m, 2H, aromatic), 7.12–7.17 (m, 2H, aromatic), 7.26–7.28 (m, 3H, aromatic), 9.12 (s, 1H, NH), ^{13}C-NMR (100 MHz, DMSO-d_6): δ (ppm) 26.84, 27.36, 29.30, 29.57, 32.64, 35.26, 35.47, 45.81, 50.70, 65.20, 103.35, 103.49, 110.51, 110.68, 127.95, 128.12, 128.71, 137.10, 145.10, 145.30, 146.37, 149.79, 150.00, 167.16, 194.88.

Dibenzyl4,4′-((hexane-1,6-diylbis(oxy))bis(2,1-phenylene))bis(2,7,7-trimethyl-5-oxo-1,4,5,6,7,8-hexahydroquinoline-3-carboxylate) (Table 5, Entry24, Figures S23 and S24)

Solid, m.p.161–163 °C. ^{1}H NMR (300 MHz, DMSO-d6): δ = 0.84 (s, 3H, CH$_3$), 1.00 (s, 3H, CH$_3$), 1.49 (br, 2H, CH$_2$ bridge), 1.72 (br, 2H, CH$_2$ bridge), 1.90 (d,1H, J = 16 Hz, CH$_2$), 2.13–2.39 (m, 5H, J = 18 Hz, CH$_2$, CH$_3$), 2.48 (d, 1H, J = 16 Hz CH$_2$), 3.82 (dd, 2H, J = 7.2, 38.4 Hz OCH$_2$ bridge), 4.97 (AB q, 2H, J = 12 Hz, OCH$_2$), 5.08 (s, 1H, benzlic), 6.68–6.84 (m, 2H, aromatic), 7.03–7.29 (m, 7H, aromatic), 9.02 (s, 1H, NH), ^{13}C NMR(300 MHz, DMSO-d_6): δ = 18.92, 26.13, 26.63, 29.71, 29.83, 32.40, 34.77, 50.87, 64.99, 67.93, 102.59, 109.29, 112.10, 119.57, 127.44, 128.04, 128.13, 128.66, 132.09, 134.71, 137.33, 145.50, 150.05, 157.57, 167.53, 194.37 ppm.

3. Experimental Section

3.1. Materials

Paraphenylenediamine (*p*PDA), ammonium persulfate (APS), pyridine, sulfuric acid, dimedone, Iron (II), and (III) slats, benzyl acetoacetate, ammonium acetate, DPPH (2,2-diphenyl-1-picrylhydrazyl) radical scavenging, and all employed solvents were provided by Merck company (Germany).
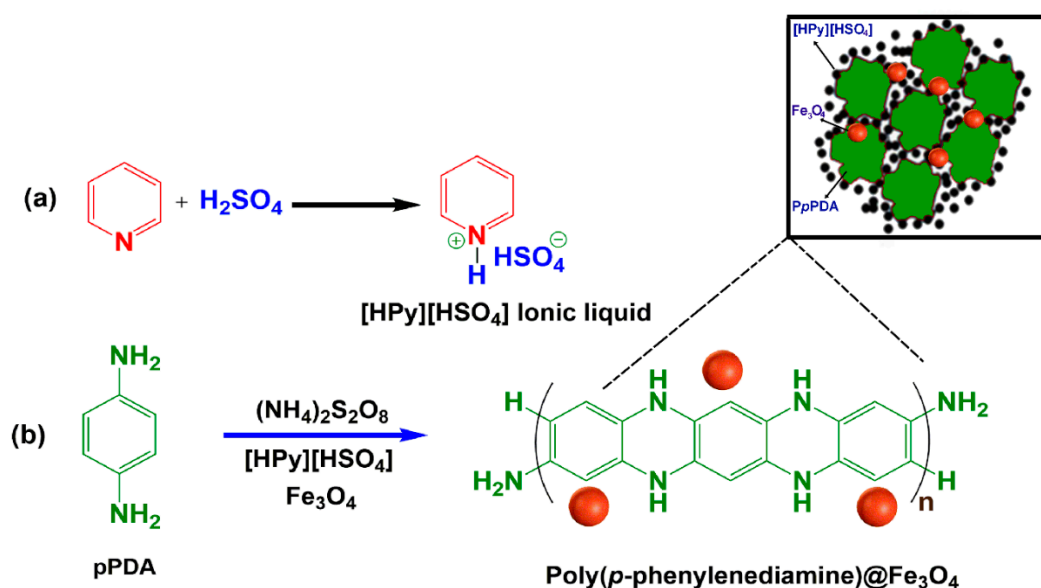
3.2. Preparation of Iron Oxide Nanoparticles

Iron oxide nanoparticles (Fe$_3$O$_4$ NPs) were prepared by the co-precipitation technique as follows [40]. FeCl$_3$·6H$_2$O (2.73 g) and FeCl$_2$·4H$_2$O (0.99 g) were dissolved in deionized water at ambient temperature, and then 10 mL ammonia solution (25%) was added into the above solution under constant stirring for a half-hour, and the final pH was 10. Lastly, the black precipitate was isolated by a magnet and washed with distilled water and ethanol, and dried at 80 °C under vacuum for 2 h.

3.3. Pyridinium Hydrogen Sulfate [HPy][HSO$_4$] Preparation

Pyridinium hydrogen sulfate [HPy][HSO$_4$] was prepared as follows (Scheme 2a) [41]. 10 mL of pyridine was poured into a flask, then 6.76 mL of sulfuric acid solution was added slowly into pyridine for one hour under stirring at 0–5 °C. Afterward, the solution was

maintained for 5 h at 0–5 °C to complete the reaction. Lastly, water was removed by a rotary evaporator to give a colorless liquid.

Scheme 2. Preparation of (**a**) [HPy][HSO$_4$] and (**b**) PpPDA@Fe$_3$O$_4$ nanocomposite in the presence of [HPy][HSO$_4$]. Note: The relative size of nanoparticles and chemical structures in the scheme is assumptive.

3.4. Fabrication of Poly(p-Phenylenediamine)@Fe₃O₄ in [HPy][HSO₄] Ionic Liquid

The magnetic poly(p-phenylenediamine)@Fe$_3$O$_4$ (PpPDA@Fe$_3$O$_4$) was fabricated through the in-situ chemical oxidative polymerization in presence of iron oxide nanoparticles and [HPy][HSO$_4$] ionic liquid as follows:

1 g of pPDA monomer was dissolved in the 30 mL of distilled water under constant stirring at room temperature and then 9.24 mmol of [HPy][HSO$_4$] (optimized amount) was added to the solution. In a separate beaker, iron oxide nanoparticles (0.05 g) in 15 mL of distilled water were dispersed under ultrasonic irradiation for 30 min. Then, the iron oxide nanoparticles mixture was added to the above solution. The polymerization was initiated by the addition of 10 mL of the ammonium persulfate solution (0.99 mol/L) under constant stirring at room temperature. The mixture was retained under constant stirring at room temperature for 24 h. The precipitate was collected by the external magnet and washed with deionized water and methanol and dried at 70° for 24 h (Scheme 2b). For a better comparison of the catalytic activity of nanocomposite, PpPDAs in the presence and absence of [HPy][HSO$_4$] were also synthesized according to the above procedure.

3.5. Overall Route for the Synthesis of Polyhydroquinoline Derivatives

One-pot synthesis of polyhydroquinoline compounds was carried out as follows:

A mixture of dimedone (1.0 mmol), aldehyde (1.0 mmol), benzyl acetoacetate (1.0 mmol), ammonium acetate (1.0 mmol), and PpPDA@Fe$_3$O$_4$ (0.04 g) in ethanol solvent (5 mL) was refluxed. Rection was traced by thin-layer chromatography (hexane/ethyl acetate 5:1). Once the reaction was completed the catalyst was separated easily by an external magnet. Afterward, the crude solid product was filtered and then purified by recrystallization from ethanol.

3.6. Antioxidant Activity

Antioxidant activity evaluation of prepared materials was studied in ethanolic DPPH solution (25 μM/L) by a UV-vis spectroscopy. The amount of each sample (10 mg) was

added to tubes containing2 mL of ethanolic DPPH and then the tubes were kept in a dark place for 6 h. After that, DPPH inhibition (%) was measured by the following Equation:

$$\text{DPPH inhibition (\%)} = (A_b - A_s)/A_b \times 100 \qquad (1)$$

In this equation, A_b and A_s are the absorption of DPPH solution and samples at 517 nm, respectively.

3.7. Antibacterial Activity

Kirby–Bauer disc diffusion technique was employed for antibacterial activities study of the prepared samples. Sample solutions (20 mg in 10 mL dimethyl sulfoxide, DMSO) were filtered by a Ministart (Sartorius). The antibacterial activity of the samples was evaluated against *Bacillus subtilis* PTCC 1023 (Gram-positive) and *Escherichia coli* PTCC 1330 (Gram-negative) bacterial species. The bacteria phase was prepared via inoculating of the cultures 1% (*v/v*) into the Muller–Hinton broth and incubating on a shaker at 37 °C for 24 h. Sterile paper discs were soaked with 10 µL of the sample solutions then allowed to dry. The soaked discs were placed on the agar plate and incubated at 37 °C for 24 h. The antibacterial activities of the compounds were compared with gentamicin and chloramphenicol antibiotics as positive control and DMSO as a negative control. Antibacterial activity was studied by evaluating the inhibition zone diameter (mm) of the surface of the plates and the results were reported as Mean $\pm$ SD after three repeats.

3.8. Characterization

The chemical structure of the synthesized materials was investigated by a Fourier transform infrared spectroscopy (FTIR) (Bruker Tensor 27, Bremen, Germany), hydrogen and carbon nuclear magnetic resonance spectroscopy (^{1}HNMR and ^{13}CNMR) (Bruker Avance DRX-400, Bremen, Germany), elemental analysis (CHNS) (Costech-Italy) and energy dispersive X-ray (EDX) (MIRA 3-XMU, Brno, Czech Republic). The surface morphology and crystallinity of products were evaluated by field emission scanning electron microscopy (FESEM) (MIRA 3-XMU, Czech Republic) and X-ray diffraction (XRD) (BrukerD8 Advance X-ray diffractometer, Bremen, Germany), respectively.

4. Conclusions

Antibacterial and antioxidant P*p*PDA@Fe$_3$O$_4$ nanocomposite was successfully fabricated by in-situ oxidative polymerization in the presence of [HPy][HSO$_4$] and iron oxide nanoparticles as a potential heterogeneous nanocatalyst for the synthesis of polyhydroquinolines derivatives. The nanocatalyst was characterized by different techniques and results displayed that the nanocatalyst showed superparamagnetic behavior with crystalline nature. The solubility test showed that prepared P*p*PDA in presence of [HPy][HSO$_4$] had better solubility than PpPDA. The P*p*PDA@Fe$_3$O$_4$ nanocatalyst showed good antibacterial activity against *Escherichia coli* and *Bacillus subtilis*. The FESEM of nanocatalyst showed the hexagonal structure with a high agglomerate with a diameter of ~100 nm. The P*p*PDA@Fe$_3$O$_4$ nanocatalyst showed great catalytic performance in the synthesis of polyhydroquinolines derivatives and the corresponding products were synthesized with high yield (90–97%) without a difficult work-up procedure. Moreover, the P*p*PDA@Fe$_3$O$_4$ nanocatalyst separated easily from the reaction media by a magnet. Reusability results showed that the nanocatalyst could use for at least five times without a significant decrease in catalytic activity. According to the proposed mechanistic scheme, the prepared P*p*PDA@Fe$_3$O$_4$ nanocatalyst in [HPy][HSO$_4$] played an important role in directing the synthesis reaction of polyhydroquinolines derivatives with favorable features, e.g., Brønsted acid, strong basic sites, and high surface area. It could be concluded the bioactive P*p*PDA@Fe$_3$O$_4$ nanocomposite could be employed as an eco-friendly and high efficiency nanocatalyst for the synthesis of different organic reactions. P*p*PDA@Fe$_3$O$_4$ nanocatalysts and 11 polyhydroquinolines derivatives showed antioxidant activity between 75% and

99%. Among polyhydroquinolines derivatives, only 5r and 5v had good growth inhibitory effects against tested microorganisms.

Supplementary Materials: The following supporting information can be downloaded. Figure S1: ^{1}H-NMR spectra of benzyl 2,7,7-trimethyl-4-(4-nitrophenyl)-5-oxo-1,4,5,6,7,8-hexahydroquinoline-3-carboxylate (Table 5, Entry2), Figure S2: ^{13}C-NMR spectra of benzyl 2,7,7-trimethyl-4-(4-nitrophenyl)-5-oxo-1,4,5,6,7,8-hexahydroquinoline-3-carboxylate (Table 5, Entry2), Figure S3: ^{1}H-NMR spectra of Benzyl¬4-(3-ethoxy-4-hydroxyphenyl)-2,7,7-trimethyl-5-oxo-1,4,5,6,7,8-hexahy¬droquino line -3-carboxylate (Table 5, Entry 3), Figure S4: ^{13}C-NMR spectra of Benzyl¬4-(3-ethoxy-4-hydroxyphenyl)-2,7,7-trimethyl-5-oxo-1,4,5,6,7,8-hexahy¬droquino line -3-carboxylate (Table 5, Entry 3), Figure S5: ^{1}H-NMR spectra of benzyl 2,7,7-trimethyl-5-oxo-4-(3,4,5-trimethoxyphenyl)-1,4,5,6,7,8-hexahydroquinoline-3-carboxylate (Table 5, Entry 5), Figure S6: ^{13}C-NMR spectra of benzyl 2,7,7-trimethyl-5-oxo-4-(3,4,5-trimethoxyphenyl)-1,4,5,6,7,8-hexahydroquinoline-3-carboxylate (Table 5, Entry 5), Figure S7: ^{1}H-NMR spectra of Benzyl¬2,7,7-trimethyl-5-oxo-4-(p-tolyl)-1,4,5,6,7,8-hexahydroquinoline-3-carboxylate (Table 5, Entry 9), Figure S8: ^{13}C-NMR spectra of Benzyl¬2,7,7-trimethyl-5-oxo-4-(p-tolyl)-1,4,5,6,7,8-hexahydroquinoline-3-carboxylate (Table 5, Entry 9), Figure S9: ^{1}H-NMR spectra of Benzyl 2,7,7-trimethyl-4-(4-(methylthio)phenyl)-5-oxo-1,4,5,6,7,8-hexahydroquinoline-3-carboxylate (Table 5, Entry10), Figure S10: ^{13}C-NMR spectra of Benzyl 2,7,7-trimethyl-4-(4-(methylthio)phenyl)-5-oxo-1,4,5,6,7,8-hexahydroquinoline-3-carboxylate (Table 5, Entry10), Figure S11: ^{1}H-NMR spectra of benzyl 4-(4-ethylphenyl)-2,7,7-trimethyl-5-oxo-1,4,5,6,7,8-hexahydroquinoline-3-carboxylate (Table 5, Entry 13), Figure S12: ^{13}C-NMR spectra of benzyl 4-(4-ethylphenyl)-2,7,7-trimethyl-5-oxo-1,4,5,6,7,8-hexahydroquinoline-3-carboxylate(Table 5, Entry 13), Figure S13: ^{1}H-NMR spectra of Benzyl 4-(3,4-dimethoxyphenyl)-2,7,7-trimethyl-5-oxo-1,4,5,6,7,8-hexahydroquinoline-3-carboxylate (Table 5, Entry15), Figure S14: ^{1}H-NMR spectra of benzyl 4-(2-chlorophenyl)-2,7,7-trimethyl-5-oxo-1,4,5,6,7,8-hexahydroquinoline-3-carboxylate (Table 5, Entry 18), Figure S15: ^{13}C-NMR spectra of benzyl 4-(2-chlorophenyl)-2,7,7-trimethyl-5-oxo-1,4,5,6,7,8-hexahydroquinoline-3-carboxylate (Table 5, Entry 18), Figure S16: ^{1}H-NMR spectra of benzyl 4-(3-hydroxyphenyl)-2,7,7-trimethyl-5-oxo-1,4,5,6,7,8-hexahydroquinoline-3-carboxylate (Table 5, Entry 19), Figure S17: ^{13}C-NMR spectra of benzyl 4-(3-hydroxyphenyl)-2,7,7-trimethyl-5-oxo-1,4,5,6,7,8-hexahydroquinoline-3-carboxylate (Table 5, Entry 19), Figure S18: ^{1}H-NMR spectra of benzyl 4-(2-hydroxy-3-methoxyphenyl)-2,7,7-trimethyl-5-oxo-1,4,5,6,7,8-hexahydroquinoline-3-carboxylate (Table 5, Entry 20), Figure S19: ^{13}C-NMR spectra of benzyl 4-(3-hydroxy-4-methoxyphenyl)-2,7,7-trimethyl-5-oxo-1,4,5,6,7,8-hexahydroquinoline-3-carboxylate (Table 5, Entry 20), Figure S20: ^{1}H-NMR spectra of benzyl 4-(3-hydroxy-4-methoxyphenyl)-2,7,7-trimethyl-5-oxo-1,4,5,6,7,8-hexahydroquinoline-3-carboxylate (Table 5, Entry22), Figure S21: ^{1}H-NMR spectra of dibenzyl 4,4′-(1,4-phenylene)bis(2,7,7-trimethyl-5-oxo-1,4,5,6,7,8-hexahydroquinoline-3-carboxylate) (Table 5, Entry23), Figure S22: ^{13}C-NMR spectra of dibenzyl 4,4′-(1,4-phenylene)bis(2,7,7-trimethyl-5-oxo-1,4,5,6,7,8-hexahydroquinoline-3-carboxylate) (Table 5, Entry 23), Figure S23: ^{1}H-NMR spectra of Dibenzyl 4,4′-((hexane-1,6-diylbis(oxy))bis(2,1-phenylene))bis(2,7,7-trimethyl-5-oxo-1,4,5,6,7,8-hexahydroquinoline-3-carboxylate) (Table 5, Entry24), Figure S24: ^{13}C-NMR Spectra of dibenzyl 4,4′-((hexane-1,6-diylbis(oxy))bis(2,1-phenylene))bis(2,7,7-trimethyl-5-oxo-1,4,5,6,7,8-hexahydroquinoline-3-carboxylate) (Table 5, Entry24).

Author Contributions: Methodology, S.M.N. and A.D.; investigation, S.M.N.; writing—original draft preparation, E.N.Z.; writing—review and editing, E.N.Z., S.A.P., M.A. and A.P.K.; supervision, E.N.Z.; project administration, E.N.Z. and S.A.P. All authors have read and agreed to the published version of the manuscript.

Conflicts of Interest: The authors declare no conflict of interest.

References

1. Xu, P.; Liang, S.; Zong, M.-H.; Lou, W.-Y. Ionic liquids for regulating biocatalytic process: Achievements and perspectives. *Biotechnol. Adv.* **2021**, *51*, 107702. [CrossRef] [PubMed]
2. Cull, S.G.; Holbrey, J.D.; Vargas-Mora, V.; Seddon, K.R.; Lye, G.J. Room-temperature ionic liquids as replacements for organic solvents in multiphase bioprocess operations. *Biotechnol. Bioeng.* **2000**, *69*, 227–233. [CrossRef]
3. Erbeldinger, M.; Mesiano, A.J.; Russell, A.J. Enzymatic catalysis of formation of Z-aspartame in ionic liquid−an alternative to enzymatic catalysis in organic solvents. *Biotechnol. Prog.* **2000**, *16*, 1129–1131. [CrossRef] [PubMed]
4. Egorova, K.S.; Posvyatenko, A.V.; Larin, S.S.; Ananikov, V.P. Ionic liquids: Prospects for nucleic acid handling and delivery. *Nucleic Acids Res.* **2021**, *49*, 1201–1234. [CrossRef] [PubMed]
5. Egorova, K.S.; Gordeev, E.G.; Ananikov, V.P. Biological Activity of Ionic Liquids and Their Application in Pharmaceutics and Medicine. *Chem. Rev.* **2017**, *117*, 7132–7189. [CrossRef]
6. Abbott, A.P.; McKenzie, K.J. Application of ionic liquids to the electrodeposition of metals. *Phys. Chem. Chem. Phys.* **2006**, *8*, 4265–4279. [CrossRef] [PubMed]
7. Hallett, J.P.; Welton, T. Room-temperature ionic liquids: Solvents for synthesis and catalysis. 2. *Chem. Rev.* **2011**, *111*, 3508–3576. [CrossRef]
8. Pahovnik, D.; Žagar, E.; Kogej, K.; Vohlídal, J.; Žigon, M. Polyaniline nanostructures prepared in acidic aqueous solutions of ionic liquids acting as soft templates. *Eur. Polym. J.* **2013**, *49*, 1381–1390. [CrossRef]
9. Harun, M.H.; Saion, E.; Kassim, A.; Yahya, N.; Mahmud, E. Conjugated Conducting Polymers: A Brief Overview. *Sens. Peterbrgh. NH* **2007**, *2*, 63–68.
10. Zare, E.N.; Agarwal, T.; Zarepour, A.; Pinelli, F.; Zarrabi, A.; Rossi, F.; Ashrafizadeh, M.; Maleki, A.; Shahbazi, M.-A.; Maiti, T.K. Electroconductive multi-functional polypyrrole composites for biomedical applications. *Appl. Mater. Today* **2021**, *24*, 101117. [CrossRef]
11. Zare, E.N.; Lakouraj, M.M.; Ashna, A. Synthesis of conductive poly (3-aminobenzoic acid) nanostructures with different shapes in acidic ionic liquids medium. *J. Mol. Liq.* **2018**, *271*, 514–521. [CrossRef]
12. Zare, E.N.; Motahari, A.; Sillanpää, M. Nanoadsorbents based on conducting polymer nanocomposites with main focus on polyaniline and its derivatives for removal of heavy metal ions/dyes: A review. *Environ. Res.* **2018**, *162*, 173–195. [CrossRef] [PubMed]
13. Donescu, D.; Fierascu, R.C.; Ghiurea, M.; Manaila-Maximean, D.; Nicolae, C.A.; Somoghi, R.; Spataru, C.I.; Stanica, N.; Raditoiu, V.; Vasile, E. Synthesis and magnetic properties of inverted core-shell polyaniline-ferrite composite. *Appl. Surf. Sci.* **2017**, *414*, 8–17. [CrossRef]
14. Zare, E.N.; Makvandi, P.; Ashtari, B.; Rossi, F.; Motahari, A.; Perale, G. Progress in Conductive Polyaniline-Based Nanocomposites for Biomedical Applications: A Review. *J. Med. Chem.* **2020**, *63*, 1–22. [CrossRef]
15. Livi, S.; Gérard, J.F.; Duchet-Rumeau, J. Ionic liquids as polymer additives. In *Applications of Ionic Liquids in Polymer Science and Technology*; Mecerreyes, D., Ed.; Springer: Berlin/Heidelberg, Germany, 2015; pp. 1–21, ISBN 9783662449035.
16. Krishna, A.; Laslau, C.; Waterhouse, G.I.N.; Zujovic, Z.D.; Travas-Sejdic, J. Effect of ionic liquid on polyaniline chemically synthesised under falling-pH conditions. *Chem. Pap.* **2013**, *67*, 995–1001. [CrossRef]
17. Miao, Z.; Wang, Y.; Liu, Z.; Huang, J.; Han, B.; Sun, Z.; Du, J. Synthesis of polyaniline nanofibrous networks with the aid of an amphiphilic ionic liquid. *J. Nanosci. Nanotechnol.* **2006**, *6*, 227–230. [CrossRef]
18. Arias, L.S.; Pessan, J.P.; Vieira, A.P.M.; De Lima, T.M.T.; Delbem, A.C.B.; Monteiro, D.R. Iron oxide nanoparticles for biomedical applications: A perspective on synthesis, drugs, antimicrobial activity, and toxicity. *Antibiotics* **2018**, *7*, 46. [CrossRef]
19. Bahadorikhalili, S.; Ma'mani, L.; Mahdavi, H.; Shafiee, A. Palladium catalyst supported on PEGylated imidazolium based phosphinite ionic liquid-modified magnetic silica core–shell nanoparticles: A worthy and highly water-dispersible catalyst for organic reactions in water. *RSC Adv.* **2015**, *5*, 71297–71305. [CrossRef]
20. Eivazzadeh-Keihan, R.; Maleki, A. Design and synthesis of a new magnetic aromatic organo-silane star polymer with unique nanoplate morphology and hyperthermia application. *J. Nanostructure Chem.* **2021**, *11*, 751–767. [CrossRef]
21. Marzouk, A.A.; Abu-Dief, A.M.; Abdelhamid, A.A. Hydrothermal preparation and characterization of ZnFe2O4 magnetic nanoparticles as an efficient heterogeneous catalyst for the synthesis of multi-substituted imidazoles and study of their anti-inflammatory activity. *Appl. Organomet. Chem.* **2018**, *32*, e3794. [CrossRef]
22. Babudurai, M.; Nwakanma, O.; Romero-Nuñez, A.; Manisekaran, R.; Subramaniam, V.; Castaneda, H.; Jantrania, A. Mechanical activation of TiO2/Fe2O3 nanocomposite for arsenic adsorption: Effect of ball-to-powder ratio and milling time. *J. Nanostructure Chem.* **2021**, *11*, 619–632. [CrossRef]
23. Halim, E.M.; Perrot, H.; Sel, O.; Debiemme-Chouvy, C.; Lafdi, K.; El Rhazi, M. Electrosynthesis of hierarchical Cu2O–Cu(OH)2 nanodendrites supported on carbon nanofibers/poly(para-phenylenediamine) nanocomposite as high-efficiency catalysts for methanol electrooxidation. *Int. J. Hydrog. Energy* **2021**, *46*, 19926–19938. [CrossRef]
24. Su, X.; Yao, Y.; Tian, J.; Liu, J.; Wang, Z.; You, Y.; Huang, L.; Wu, C. Investigation of the durability of a poly-p-phenylenediamine/carbon black composite for the oxygen reduction reaction. *Chin. J. Catal.* **2016**, *37*, 1096–1102. [CrossRef]
25. Mirzaei-Mosbat, M.; Ghorbani-Vaghei, R.; Karamshahi, Z. Layered double hydroxides@poly(p-phenylenediamine)@Cu as a novel catalyst for the synthesis of pyrrole derivatives: Preparation and characterization. *Res. Chem. Intermed.* **2020**, *46*, 1613–1628. [CrossRef]

26. Karamshahi, Z.; Ghorbani-Vaghei, R. Facile synthesis of indolizines using layered double hydroxides@poly(p-phenylenediamine) as a catalyst with a green tool (neat technology). *Appl. Organomet. Chem.* **2020**, *34*, e5347. [CrossRef]

27. Ortiz, M.E.; Núñez-Vergara, L.J.; Camargo, C.; Squella, J.A. Oxidation of Hantzsch 1, 4-dihydropyridines of pharmacological significance by electrogenerated superoxide. *Pharm. Res.* **2004**, *21*, 428–435. [CrossRef]

28. Bossert, F.; Meyer, H.; Wehinger, E. 4-Aryldihydropyridines, a New Class of Highly Active Calcium Antagonists. *Angew. Chem. Int. Ed.* **1981**, *20*, 762–769. [CrossRef]

29. Kazemi, M.; Mohammadi, M. Magnetically Recoverable Catalysts: Catalysis in Synthesis of Polyhydroquinolines. *Appl. Organomet. Chem.* **2020**, *34*, 42–48. [CrossRef]

30. Ahankar, H.; Ramazani, A.; Joo, S.W. Magnetic nickel ferrite nanoparticles as an efficient catalyst for the preparation of polyhydroquinoline derivatives under microwave irradiation in solvent-free conditions. *Res. Chem. Intermed.* **2016**, *42*, 2487–2500. [CrossRef]

31. Balaji, G.L.; Rajesh, K.; Venkatesh, M.; Sarveswari, S.; Vijayakumar, V. Ultrasound-promoted synthesis of bi-, tri- and tetrapodal polyhydroquinolines, 1,4-dihydropyridines and the corresponding pyridines. *RSC Adv.* **2014**, *4*, 39–46. [CrossRef]

32. Amer, I.; Brandt, S. Synthesis and characterization of Poly(p-phenylenediamine) and its derivatives using aluminium triflate as a co-catalyst. *Cogent Eng.* **2018**, *5*, 1499701. [CrossRef]

33. Arya, V.; Philip, L. Adsorption of pharmaceuticals in water using Fe_3O_4 coated polymer clay composite. *Microporous Mesoporous Mater.* **2016**, *232*, 273–280. [CrossRef]

34. Muhammad, A.; Bilal, S. Comparative study of the adsorption of Acid Blue 40 on polyaniline, magnetic oxide and their composites: Synthesis, characterization and application. *Materials* **2019**, *12*, 2854. [CrossRef] [PubMed]

35. Loh, K.-S.; Lee, Y.H.; Musa, A.; Salmah, A.A.; Zamri, I. Use of Fe_3O_4 nanoparticles for enhancement of biosensor response to the herbicide 2, 4-dichlorophenoxyacetic acid. *Sensors* **2008**, *8*, 5775–5791. [CrossRef] [PubMed]

36. Davarpanah, A.; Zare, E.N.; Zamani, M. Acidic ionic liquid-mediated preparation of shaped electrically conductive poly (p-phenylenediamine). *J. Polym. Res.* **2021**, *28*, 224. [CrossRef]

37. Mathew, J.; Sathishkumar, M.; Kothurkar, N.K.; Senthilkumar, R.; Narayanan, B.S. Polyaniline/Fe_3O_4-RGO nanocomposites for microwave absorption. In *IOP Conference Series: Materials Science and Engineering*; IOP Publishing: Bristol, UK, 2018; Volume 310, p. 12138.

38. Kechrakos, D.; Trohidou, K.N. Magnetic properties of dipolar interacting single-domain particles. *Phys. Rev. B* **1998**, *58*, 12169. [CrossRef]

39. Behbahani, F.K.; Homafar, M. Synthesis of polyhydroquinoline derivatives through the hantzsch four component using iron (III) phosphate as a catalyst. *Synth. React. Inorg. Met. Nano-Metal Chem.* **2012**, *42*, 291–295. [CrossRef]

40. Wu, S.; Sun, A.; Zhai, F.; Wang, J.; Xu, W.; Zhang, Q.; Volinsky, A.A. Fe_3O_4 magnetic nanoparticles synthesis from tailings by ultrasonic chemical co-precipitation. *Mater. Lett.* **2011**, *65*, 1882–1884. [CrossRef]

41. Tao, D.J.; Wu, Y.T.; Zhou, Z.; Geng, J.; Hu, X.B.; Zhang, Z.B. Kinetics for the esterification reaction of n -butanol with acetic acid catalyzed by noncorrosive brønsted acidic ionic liquids. *Ind. Eng. Chem. Res.* **2011**, *50*, 1989–1996. [CrossRef]